J Mater Sci (2010) 45:6115–6125
DOI 10.1007/s10853-010-4698-7

Study of the effect of prolonged magnetic stirring on the physico-chemical surface properties of nanometric transition alumina

B. Bonelli · P. Palmero · F. Lomello · M. Armandi · M. Lombardi

Received: 15 January 2010 / Accepted: 7 June 2010 / Published online: 17 June 2010

Abstract This article reports the study of a transition nanometric alumina both as such and after prolonged magnetic stirring in bi-distilled water. Stirring was effective in inducing a significant reduction of starting particles agglomeration and modification of the surface properties of the material. The formation of an $Al(OH)_3$ (gibbsite) phase after magnetic stirring in water was detected by means of XRD on powdered samples. Correspondingly, Infra Red spectrum of magnetically stirred alumina outgassed at 150 °C showed a band at ca. 3300 cm^{-1}, ascribable to the hydroxide phase, which decomposes at higher temperature. Differential thermal analysis and thermogravimetry also showed a different thermal behaviour between the two materials, in that magnetically stirred alumina presents a broad endothermic peak at about 280 °C accompanied by an abrupt mass loss (ca. 0.5% of the initial weight), due to dehydration of the hydroxide phase.

Introduction

The term 'alumina' refers to different materials: the thermodynamically stable corundum phase (α-Al_2O_3), of paramount importance in the field of ceramic applications, is the ultimate product of treatment at $T \geq 1{,}400$ K of all Al oxidic and hydrated systems [1]. In catalysis and surface chemistry, the term alumina is usually referred to the so-called 'transition aluminas', which are metastable phases of low crystallinity with high surface area and open porosity [2].

The attention is nowadays focused on nanostructured ceramics, implying the use of ultra-fine powders, which can offer a variety of attractive properties, such as enhanced sinterability as compared to corresponding coarse-grained ones [3]. Nano-sized ceramic powders, however, can often exhibit soft and/or hard agglomeration, the former due to weak van der Waals interactions between particles, the latter referring to primary particles strongly bound together as a result of neck growth. Soft agglomerates can be normally broken by simple mechanical stirring, low-energy agitation or ultra-sonication [4], while for hard agglomerates higher stresses are needed, requiring high-energy milling or high shear mixing processes [4]. The dry forming of hard agglomerated powders leads to green microstructures which are affected by two types of pores: micronic inter-agglomerates pores, and nanometric inter-crystallites ones, within the agglomerate itself. During sintering, the elimination of inter-agglomerates pores needs high temperatures, thus encouraging grain growth [5]. As a matter of fact, agglomeration-free particles and narrow size distributions are imperative requirements for nanosized powders to be consolidated into highly dense, fine microstructures [6].

Although the ceramic industry preferentially employs α-alumina powders to manufacture fired components, the scientific interest is also focused on transition aluminas to produce fully dense alumina and alumina-based composite materials, mostly in view of developing ultra-fine, tailored microstructures [7, 8]. However, the metastability of these powders is a major drawback, since it has a critical

B. Bonelli (✉) · P. Palmero · F. Lomello · M. Armandi · M. Lombardi
Dipartimento di Scienza dei Materiali e Ingegneria Chimica, Politecnico di Torino, INSTM Research Unit PoliTO, C.so Duca degli Abruzzi 24, 10129 Torino, Italy
e-mail: barbara.bonelli@polito.it

M. Lombardi
IIT-Italian Institute of Technology @ POLITO–Centre for Space Human Robotics, C.so Trento 21, 10129 Torino, Italy

influence on their sintering behaviour. In fact, transformation into α-phase is generally accompanied by the formation of a vermicular microstructure, consisting of a network of large pores [5].

Thus, the final sintering stage requires very high firing temperatures to consolidate the material up to the theoretical density, inducing a significant grain growth. To overcome the above limitations, various approaches have been tested. For instance, wet-milling was applied to a commercial gamma alumina, demonstrating that high density samples (99%) can be produced after de-agglomeration: in fact, homogeneous and close-packed slip-cast green bodies can be yielded, able to limit the formation of the vermicular microstructure upon sintering [5]. Our previous work [9] has shown that it is possible to induce modifications of nano-crystalline transition alumina particles by dispersion, thus to lower the θ to α-alumina transformation temperature and the related activation energy. The dispersed powders also showed increased compaction behaviour under dry forming and sinterability if compared to the raw, agglomerated material [10].

So far, however, little is known about the role played by surface properties in these processes: for example, γ-Al_2O_3 when dispersed in water even at neutral pH and in the absence of other chemical species is not stable to rehydration and should be transformed back into a hydrated phase [11]. This transformation surely changes the surface properties of the material, basically the hydroxyls population [2, 12]. These microscopic effects of hydration may influence other relevant macroscopic properties, like for example the catalytic activity of γ-Al_2O_3 [13], or the material behaviour during granulation [14].

As far as the rehydration of γ-Al_2O_3 is concerned, two kinds of behaviour are reported in the literature:

(i) a hydrated layer of hydroxide $Al(OH)_3$ is formed at the surface of γ-Al_2O_3 particles after suspension in water, without dissolution of the support, due to the superficial transformation of alumina surface into aluminium hydroxide-like layers [15–20];
(ii) alumina is dissolved and then precipitated as well-shaped large $Al(OH)_3$ particles from supersaturated aqueous solution at pH $\geq$5, with a contact time between alumina and water exceeding 5 h [21].

Important factors may determine alumina surface rehydration, like contact time; pH of the aqueous solution; temperature; stirring and also the (nanometric) size of the parent material. It must be pointed out that it is also difficult to detect the hydroxide formed, since (i) whether present in small amounts, it could not be measured by XRD and (ii) although detected by XRD, its actual location (outer layer or as a separate phase) may not be unambiguously understood.

In this article, de-agglomerated transition alumina powders were obtained under magnetic stirring; this route was chosen since it brings about an effective breakage of soft agglomerates, without inducing any material pollution as occurs by other dispersion methods: ball-milling or high shear mixing in rotor–stator systems can induce, in fact, particles contamination from milling media and even phase transformation [4, 22–24]. This work reports on the effect of prolonged magnetic stirring in deionized water (pH 5.8–6.0) on commercial transition nanometric alumina, with the aims to:

(i) understand the effect of stirring on particles soft agglomeration;
(ii) study the evolution of surface functionalities as a function of rehydration and thermal treatment: the type and abundance of hydroxyls and Lewis acidic sites is indeed responsible of reactive processes at powder surface.

Experimental

Materials

A commercial, nano-crystalline transition alumina (Nanotek® by Nanophase Technologies Corporation, Darien, IL, USA), was used as starting material. The powder, hereafter referred to as A, is characterized by a purity of 99.5%, an average particle size of 47 nm and specific surface area (SSA) of 35 $m^2\ g^{-1}$, as reported by the supplier (Table 1).

Powder A was dispersed in distilled water (solid content of 50 wt%) and maintained under magnetic stirring at about 500 rpm up to 170 h, obtaining the Magnetically Stirred sample, hereafter referred to as $A_{Magnetically\ Stirred}$. pH was measured on the suspension as a function of time by a pH-meter; it was 5.1 for the as-dispersed powder and it stabilized to the value of 5.6 after 24 h of magnetic stirring, remaining almost stable up to 170 h of stirring. The measured pH value was in good agreement with literature data

Table 1 Sample A characteristics

Boiling point (°C)	2,980
Melting point (°C)	2,046
Crystal phase	δ:γ = 70:30
Average particle size (nm)	47
Purity (%)	99.5
Density (g/cm^3)	3.6
Morphology	Spherical
Specific surface area, SSA ($m^2\ g^{-1}$)	35

concerning water suspensions of γ-Al_2O_3, for which a natural pH in the 4.5–6.0 range was reported [25, 26].

Characterization techniques

The two materials were studied by means of the following techniques:

- Agglomerate size distributions were determined on powder suspensions diluted to 7 vol.% by a laser granulometer (Fritsch Analysette 22 Compact) in the 0.3–300 μm range.
- X-ray diffraction (XRD) patterns were collected on powdered samples with a Philips PW 1710 diffractometer using Cu Kα radiation (1.541874 Å), in the range 5°–70° 2θ, with a step size of 0.05° 2θ and an acquisition time per step of 5 s. Diffraction patterns were indexed by using the Powder Data File database (P.D.F. 2000, International Centre of Diffraction Data, Pennsylvania)
- Simultaneous DTA–TG analyses (Netzsch STA 409C) were performed on powdered samples of about 150 mg, up to 1,450 °C in static air, at a heating rate of 10 °C/min.
- BET (Brunauer, Emmett, Teller) SSAs of powders, previously outgassed at 150 °C for 2 h, were measured by means of N_2 adsorption/desorption isotherms at 77 K (Quantachrome Autosorb 1C instrument).
- High resolution transmission electron microscopy (HRTEM) pictures were collected on a JEOL 3010-UHR instrument, operated at 300 kV and equipped with a 2k × 2k pixel Ultrascan 100 camera. Powders were dispersed into iso-propanol and then let to dry at ambient conditions.
- For FT-IR (Fourier Transform Infra-Red) measurements, powder samples were pressed into self-supporting wafers. Spectra were collected at a resolution of 2 cm^{-1}, on a Bruker FTIR Equinox 55 spectrophotometer equipped with a MCT detector. Outgassing pretreatments were carried out using a standard vacuum frame, in a IR cell equipped with KBr windows. During outgassing treatments, residual pressure was below 1.00 * 10^{-3} mbar, as measured by a Pirani vacuum gauge. To remove water and other atmospheric contaminants, wafers were outgassed for 1 h at increasing temperatures (150, 350 and 500 °C) before adsorption of CO at nominal 77 K. Due to the weakness of the interaction with CO, adsorption is studied at low temperatures: spectra were recorded at the nominal temperature of liquid nitrogen, by dosing increasing amounts of CO (in the 0.05–15 mbar equilibrium pressures range) on samples previously outgassed at 150, 350 or 500 °C, inside a special quartz IR cell, allowing simultaneously to dose carbon monoxide and to add liquid N_2. After each experiment, an evacuation step was performed, to study the reversibility of the interaction.

Results and discussion

Effect of the magnetic stirring on particles soft agglomeration and crystalline structure

Sample A is characterized by agglomerates sizes, corresponding to 10 (d_{10}), 50 (d_{50}) and 90% (d_{90}) of the cumulative volume distribution, of 2.6, 8.0 and 16.8 μm, respectively, as determined by laser granulometry.

A significant reduction of the above soft agglomerates size was obtained under magnetic stirring of powder A water suspension. Figure 1 shows the evolution of d_{50} values as a function of the dispersion time. After 170 h of magnetic stirring, A_{MS} was obtained, whose d_{50} value was about 1 order of magnitude lower than A.

Figure 2 shows the XRD patterns of A and A_{MS} in the 5°–70° 2θ range: A is a mixture of transition alumina phases, precisely δ-Al_2O_3 (ICDD file no. 04-0877) and γ-Al_2O_3 (ICDD file no. 48-0367), as determined by XRD. Diffraction patterns of δ- and γ-phases are seen in both spectra, the only differences being the peaks at $2\theta = 18.2°$ and $2\theta = 20.3°$ (arrows) in the A_{MS} spectrum. Inset to Fig. 2 shows a detail of the 15°–25° 2θ range, in which spectra are superimposed: it is shown that the two peaks actually appear after magnetic stirring. For the sake of clarity, only the spectra of the parent material (A) and of the product obtained after 170 h of magnetic stirring (A_{MS}) are reported in the figure, but further XRD measurements on powder stirred for shorter times (namely, for 24, 36, 48 and 72 h) showed that the two peaks appear after 36 h and then their intensities remained almost constant up to 170 h.

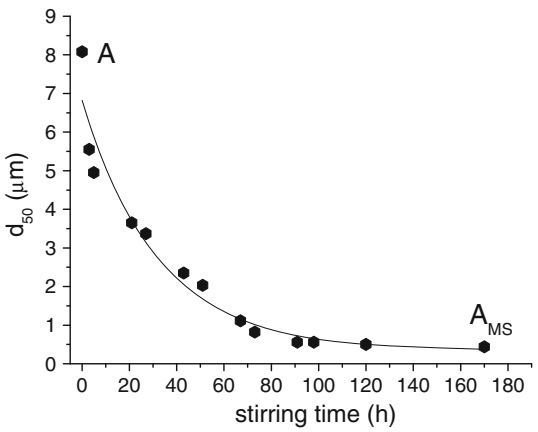

Fig. 1 Evolution of d_{50} values as a function of the dispersion time under magnetic stirring

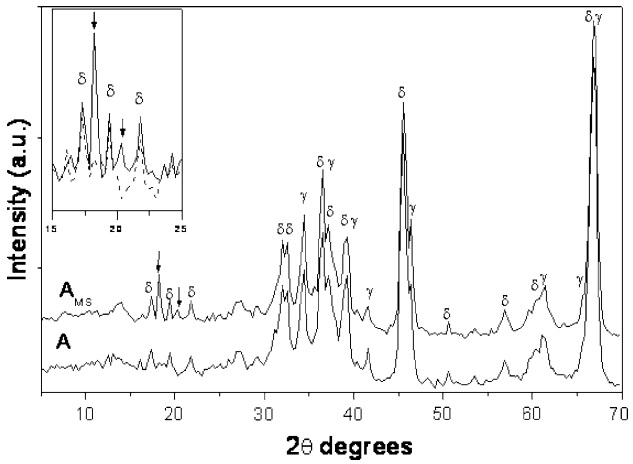

Fig. 2 XRD patterns of samples A and A_{MS} in the 5°–70° 2θ range. The inset reports a magnification of the 15°–25° 2θ range of patterns of samples A (*dashed line*) and A_{MS} (*solid line*); *arrows* point out peaks at $2\theta = 18.2°$ and $2\theta = 20.3°$ observed in the A_{MS} XRD spectrum

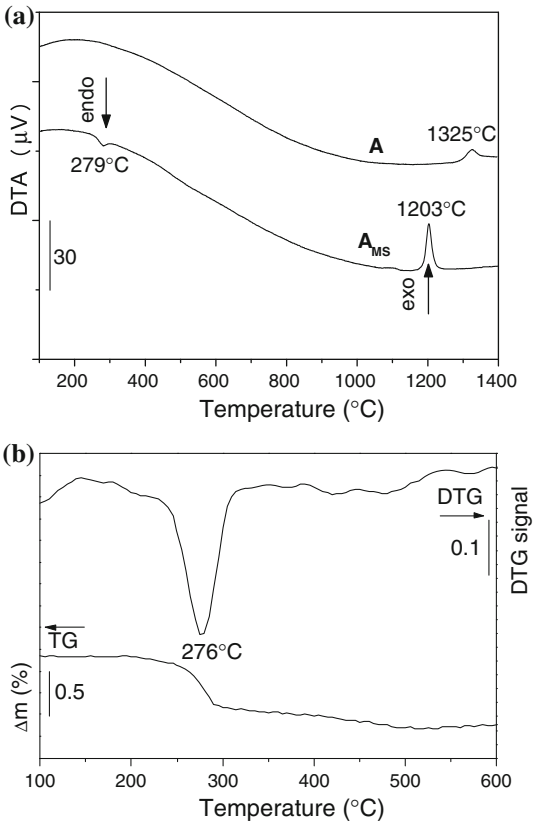

Fig. 3 DTA curves of A and A_{MS} samples (**a**); TG–DTG curves of A_{MS} in the 100–600 °C temperature range (**b**)

The two peaks are very close, in both position and relative intensity, to the (002) and (200) reflections of gibbsite, respectively (ICDD 76-1782). The two polymorphs of aluminium hydroxide $Al(OH)_3$, gibbsite and bayerite, can be, however, discriminated by the diffraction peak at about 18°, occurring at $2\theta = 18.2°$ in gibbsite and 18.8° in bayerite. The formation of a crystalline gibbsite $Al(OH)_3$ phase may thus be inferred, as a consequence of prolonged magnetic stirring in water.

This result is in agreement with literature data [21, 27], showing the formation of gibbsite [21] and bayerite [27] after suspension of γ-Al_2O_3 in water, under continuous stirring at room temperature. It is interesting to note that magnetic stirring actually plays a role in the formation of the hydroxide phase, since a blank sample prepared by suspending the powder in water for 170 h without stirring did not show any change in the XRD patterns. XRD technique, however, does not allow us to assess whether gibbsite occurs as an outer layer formed on alumina nanoparticles or as a separate phase. The fact that this phase is detected by XRD shows, however, that it is large enough to present a long range order.

The different phase composition among A and A_{MS} gave rise to different thermal behaviours upon heating, as shown by DTA curves in Fig. 3a. The dispersed powder presents, in fact, a broad endothermic peak at about 280 °C, not detectable with sample A. From TG–DTG curves of A_{MS} in the 100–600 °C range (Fig. 3b), an abrupt mass loss of about 0.5% of its initial weight was detected at the same temperature. According with XRD pattern of this sample and with literature data [21], the above thermal signal can be reasonably ascribed to gibbsite dehydration. In addition, as previously reported [9], gibbsite reflections disappeared after A_{MS} was calcined at 350 °C, thus confirming that the endothermic peak in the A_{MS} DTA curve has to be imputed to thermal decomposition of gibbsite. The amount of aluminium hydroxide formed was about 3 wt%, as estimated in a previous work from the mass-loss of water at about 280 °C in TG curve [9], the corresponding process being intermediate formation of boehmite (AlOOH) [21], and its subsequent dehydration, according to the following reactions:

$$Al(OH)_3 \rightarrow AlOOH + H_2O \quad (1)$$

$$AlOOH \rightarrow {}^1/_2\ Al_2O_3 + {}^1/_2\ H_2O \quad (2)$$

From Fig. 3a, a further difference among A and A_{MS} thermal behaviours also appears in the high temperature regime, where exothermal signals can be observed. On the ground of literature data [28, 29], these DTA peaks can be attributed to the θ to α-Al_2O_3 phase transformation, since the other lower-temperature transformations (i.e. from γ to δ and from δ to θ-alumina) do not give rise to calorimetric signal, because of topotactic transformations. They were determined at 1,325 and 1,203 °C for A and A_{MS}, respectively, denoting a significant effect of the dispersion in reducing the α-phase crystallization temperature.

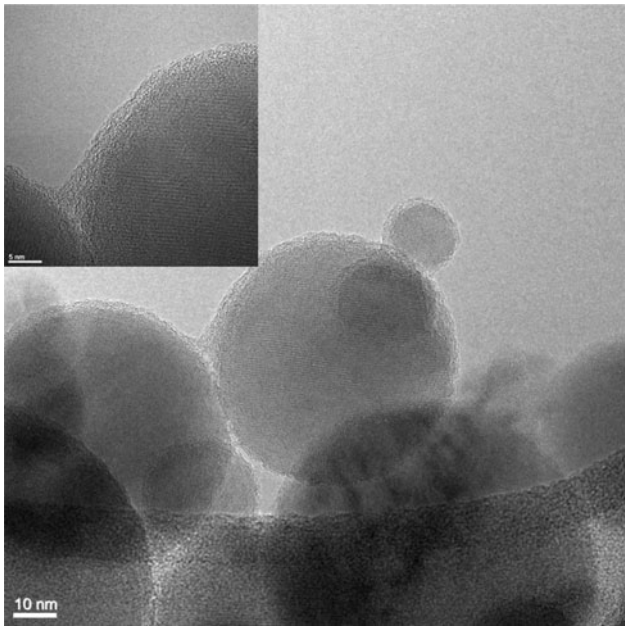

Fig. 4 Selected HRTEM picture of sample A; the inset reports a micrograph, taken at a higher magnification, showing the presence of an outer amorphous layer

HRTEM pictures were collected on A and A_{MS} powders, the latter having been dried after the pre-treatment in water: Fig. 4 shows, as an example, a selected micrograph of sample A. Both powders are composed by spherical particles of heterogeneous diameters, in the 5–100 nm range, forming agglomerates with variable size, while 'single particles' were rarely observed in both materials. The particle size analysis of the powder before and after dispersion was carried out by determining the size distribution from several micrographs of each powder sample: an average particle diameter of 35 nm was determined for both A and A_{MS}.

From HRTEM analysis it was not possible to detect any gibbsite $Al(OH)_3$ particles, unlike other works [21], reporting the formation of well-shaped gibbsite crystals separated from the alumina surface after suspension in water of nanometric γ-Al_2O_3 at varying pH. Two explanations are possible: in the first instance, HRTEM gives only a partial view of the material and in this case it was not possible to select grains in which gibbsite was observable; alternatively, the gibbsite phase may form a superficial layer, instead of distinct particles, not detectable by HRTEM observation. In this case, the micrograph taken at higher magnification (inset to Fig. 4) only shows that particles are 'covered' by a poorly ordered layer of about 2.5-nm thickness, contrasting with their well-crystallized inner part, in which the crystalline lattice fringes could be easily observed. Such amorphous layer, most probably induced by the physical vapour synthesis (PVS) of the nanostructured powders [30], seems to cover the majority of particles and will be directly in contact with water during dispersion under magnetic stirring and therefore affecting the surface properties of the final material.

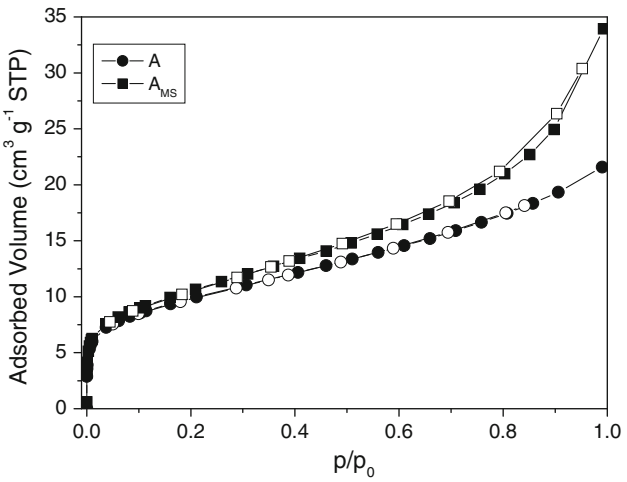

Fig. 5 N_2 adsorption/desorption isotherms at 77 K on samples A (*circles*) and A_{MS} (*squares*) out-gassed at 150 °C: *black and white symbols* refer to adsorption and desorption branch, respectively

In order to measure surface area and possible porosity, N_2 adsorption/desorption isotherms at 77 K were performed on samples previously outgassed at 150 °C, i.e. after removal of water and other surface contaminants and well before thermal decomposition of gibbsite. Figure 5 shows the corresponding curves: with both samples, Type II isotherms were obtained typical of either non-porous adsorbents or adsorbents with relatively large pores. At low p/p^0 values, Type II isotherms may resemble Type I isotherms, typical of microporous adsorbent: in this case, microporosity was evaluated by the α_s method, which showed that the occurrence of microporosity may be excluded with both powders. Most probably, the isotherm shape in the low p/p^0 range is due to high affinity between adsorbent and adsorbate, i.e. high C values in the BET equation.

The measured BET SSA values do not differ very much, in that they are 34.5 and 37.3 $m^2\ g^{-1}$ for A and A_{MS}, respectively: a good agreement is found with the surface area reported by the supplier. Magnetic stirring is shown to have a small effect on the SSA. With A_{MS} (squares), however, a limited hysteresis loop may although indicate a small change of intra-particles porosity, probably as a consequence of de-agglomeration upon long-time residence under magnetic stirring, which should also be responsible for the increase in surface area. These results show indeed that the presence of inter-particles porosity may be excluded.

Surface properties as studied by means of FT-IR spectroscopy

The species at the surface of A and A_{MS} powders were studied by means of FT-IR spectroscopy: both samples

were outgassed at increasing temperatures, namely, 150 °C (before gibbsite decomposition and after removal of atmospheric contaminants), 350 °C (after decomposition of gibbsite) and 500 °C (after severe dehydration) since the presence of surface gibbsite should give rise not only to peculiar IR bands in the hydroxyls range (3900–3000 cm^{-1}), but also to different adsorbed species and different behaviour towards thermal treatments. In order to allow comparison, all reported spectra were normalised to unit specific weight.

Figure 6a shows FT-IR spectra of sample A outgassed at 150, 350 and 500 °C: the spectrum of the sample outgassed at 150 °C shows a broad absorption in the hydroxyls stretch range (3900–3000 cm^{-1}), typical of a highly hydrated surface, due to contact with atmospheric moisture. Bands in the 1650–1200 cm^{-1} range are related to several carbonate-like species, usually observed at the surface of transition aluminas [2, 31] and definitely removed by outgassing at 500 °C.

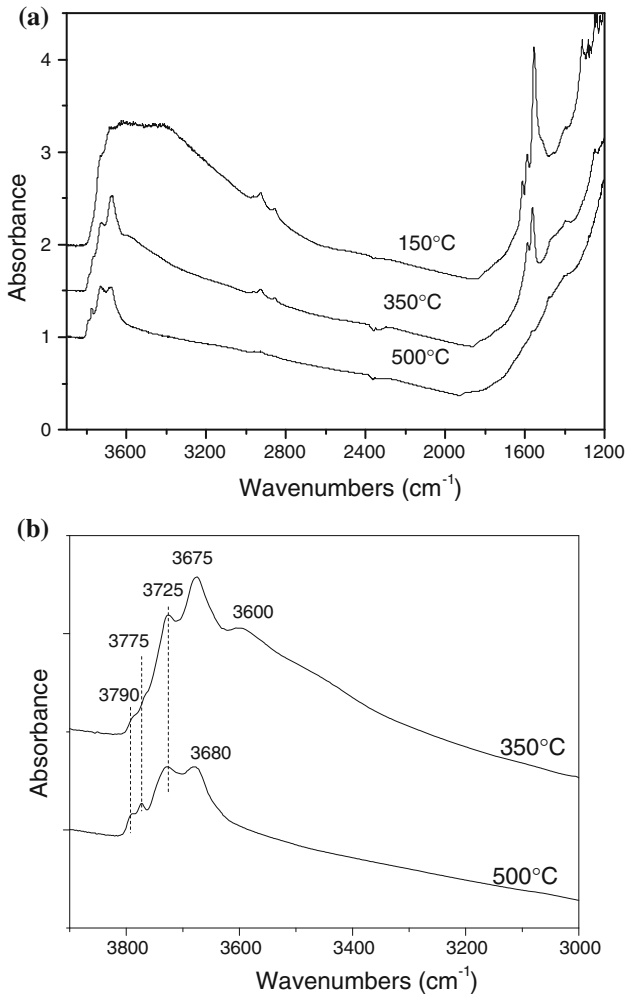

Fig. 6 FT-IR spectra recorded on sample A outgassed at 150, 350 and 500 °C (**a**). Detail of hydroxyls spectra (3900–3000 cm^{-1} range) of sample A outgassed at 350 and 500 °C (**b**)

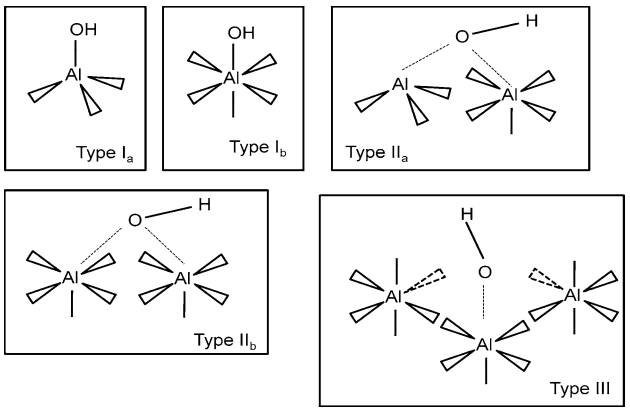

Scheme 1 Models of the different hydroxyls species at the surface of transition aluminas, after ref. [12]

Figure 6b shows a detail of hydroxyls spectra of sample A outgassed at 350 and 500 °C, showing the presence of different OH bands. In the past, several accurate models have been proposed to describe the hydroxyl population of transition aluminas [2, 12, 32–35]: in this work, reference will be made to that by Knözinger and Ratnasamy [12], depicted in Scheme 1.

Bands at 3780 and 3775 cm^{-1} are therefore assigned to type I_b and I_a hydroxyls, i.e. free terminal hydroxyls bonded to octahedral (Al^{VI}) and tetrahedral (Al^{IV}) aluminium ions, respectively; 3725 cm^{-1} band is assigned to di-bridged free OH group (type II_a) and 3675 cm^{-1} band to free hydroxyls (type III), which are tri-bridged among two octahedral (Al^{VI}) and one tetrahedral (Al^{IV}) aluminium ions; band at $\simeq$3600 cm^{-1}, with a tail on the lower wavenumbers side, is assigned H-bonded hydroxyls, which should be eliminated after outgassing at 500 °C.

Figure 7 shows FT-IR spectra of sample A_{MS} outgassed at 150, 350 and 500 °C: unlike sample A, carbonate-like species (1650–1200 cm^{-1}) are stable to thermal treatment at 500 °C, indicating that, after magnetic stirring, the surface presents stronger basic sites to which atmospheric CO_2 may coordinate, probably due to gibbsite.

These differences per se points out the effect of magnetic stirring on surface properties, but in order to allow a more detailed analysis of the type and abundance of hydroxyls in samples A and A_{MS}, Fig. 8 compare hydroxyls spectra (3900–3000 cm^{-1} range) of the two samples outgassed at 150 °C (a), 350 °C (b) and 500 °C (c).

Spectra of samples outgassed at 150 °C (Fig. 8a) are dominated by the signal of H-bonded hydroxyls (broad absorption below 3600 cm^{-1}); at higher wavenumbers, bands are seen at 3780 and 3725 cm^{-1} due to few free Al^{VI}-OH (I_b) and di-bridged OH (II_a) groups, respectively.

The stirring procedure brings about the appearance of an intense absorption at about 3330 cm^{-1} (A_{MS}), not to be

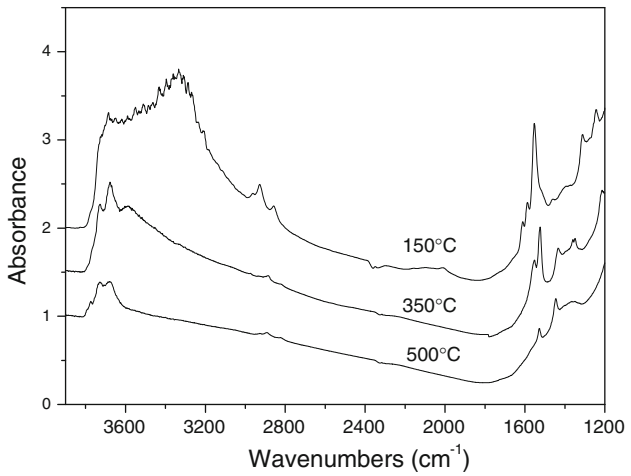

Fig. 7 FT-IR spectra recorded on sample A_{MS} outgassed at 150, 350 and 500 °C

ascribed to residual water molecules, removed at room temperature as shown in Fig. 6a.

Absorption at 3330 cm^{-1} should therefore be assigned to OH stretch mode of gibbsite hydroxyls. Gibbsite structural OH groups have been carefully studied by means of single-crystal Raman and FT-IR methods [36], which allowed authors to single out several distinct types of structural OH groups, basically inter-layer and intra-layer hydrogen bonded hydroxyls. With single crystals, authors were able to single out six ν(OH) in both IR and Raman spectra: in the present case, due to the polycrystalline nature of the material, only a new broad absorption was observed at 3330 cm^{-1}, indicating the formation of new OH species. With respect to pure gibbsite (3376 cm^{-1}) the observed frequency is lower and the band is broad, due to H-bonded OH species.

The stability of OH species was studied by increasing the outgassing temperature: as shown in Eqs. 1 and 2, $Al(OH)_3$ decomposition starts below 300 °C, to give AlOOH and Al_2O_3, and at 450 °C the transformation into γ-Al_2O_3 should be attained: for these reasons samples were out-gassed at 350 and 500 °C [2].

After outgassing at 350 °C (Fig. 8b), hydroxyls bands decrease in intensity, due to surface de-hydroxylation: the main difference between A and A_{MS} is the higher intensity of the band of H-bonded hydroxyls, which is also downward shifted, in A_{MS} (3580 cm^{-1} instead of 3600 cm^{-1}): this is indication of surface hydroxylation upon magnetic stirring.

According to Eqs. 1 and 2, after outgassing at 500 °C the typical surface features of de-hydroxylated transition alumina are expected: in Fig. 8c, bands are seen at 3790 cm^{-1} (type I_b hydroxyls), 3775 cm^{-1} (type I_a hydroxyls), 3725 cm^{-1} (type II_a hydroxyls) and 3680 cm^{-1} (type III_a hydroxyls), whereas 3580 cm^{-1} band (H-bonded hydroxyls) is removed.

Absorption intensity decreases with respect to spectra of samples treated at 150 and 350 °C, in particular as far as A_{MS} is concerned. Since normalized spectra were reported, this means that the hydrated phase, i.e. gibbsite formed upon magnetic stirring, underwent more severe de-hydroxylation upon outgassing at 500 °C.

As a whole, with the exception of 3330 cm^{-1} hydroxyls, the same OH species are present at samples surface, but with different abundance: to better address this point, CO adsorption at liquid nitrogen temperature has been studied by means of FT-IR spectroscopy.

Carbon monoxide is widely used as probe molecule to study both Lewis and Brønsted acidic sites at the surface of oxides and zeolites [2, 37–41]. When electrostatic interaction takes place between CO and the adsorbing site, like in the cases above, a hypsochromic shift occurs, with respect to free CO molecule (2143 cm^{-1}), and characteristic bands are seen in the C≡O stretch region [37]. Being the interaction very weak, low temperatures are needed and experiments are performed at the nominal temperature of liquid nitrogen.

Increasing pressures of CO (in the 0.05–30 mbar range) were dosed, at the nominal temperature of $N_{2(l)}$, on the two samples outgassed at 150, 350 and 500 °C: Figs. 9 and 10 show normalized difference spectra, obtained by subtraction of bare samples spectra shown in Fig. 8.

CO dosage on sample A outgassed at 150 °C (Fig. 9a) gives rise to the formation of (i) a main band at 2152 cm^{-1}; (ii) a weaker band in the 2189–2178 cm^{-1} range and (iii) a minor absorption at about 2107 cm^{-1}.

The 2152 cm^{-1} band is due to CO molecules interacting via H-bonding with Al^{IV}-OH species originally absorbing at 3725 cm^{-1} (in Fig. 8b), whereas 3780 cm^{-1} hydroxyls are very weak acid and do not interact with CO. The weak absorption at 2107 cm^{-1} is probably related to that at 2152 cm^{-1} and is assigned to CO molecules adsorbed through the O atom (CO–HO adducts), according to previous work [42].

The band at 2189 cm^{-1}, shifting to 2178 cm^{-1} with coverage, is assigned to CO molecules interacting with weak Lewis acidic sites, like five-coordinate Al^{3+} or, most probably, coordinatively unsaturated tetrahedral Al^{3+} of low index crystal planes [43, 44].

Figure 9b shows difference spectra recorded after CO dosage on sample A outgassed at 350 °C: two bands are seen at 2197 cm^{-1}, shifting with coverage to 2183 cm^{-1} and at 2160 cm^{-1}, shifting to 2152 cm^{-1}. The former is assigned to CO adsorbed on Al^{3+} sites forming an extended phase, the latter to CO molecules H-bonded to hydroxyls with different acidity. With respect to sample A pre-treated at 150 °C, the band of CO on Al^{3+} sites appears more intense and shifted to higher wavenumbers: this is ascribed to surface de-hydroxylation with the formation of

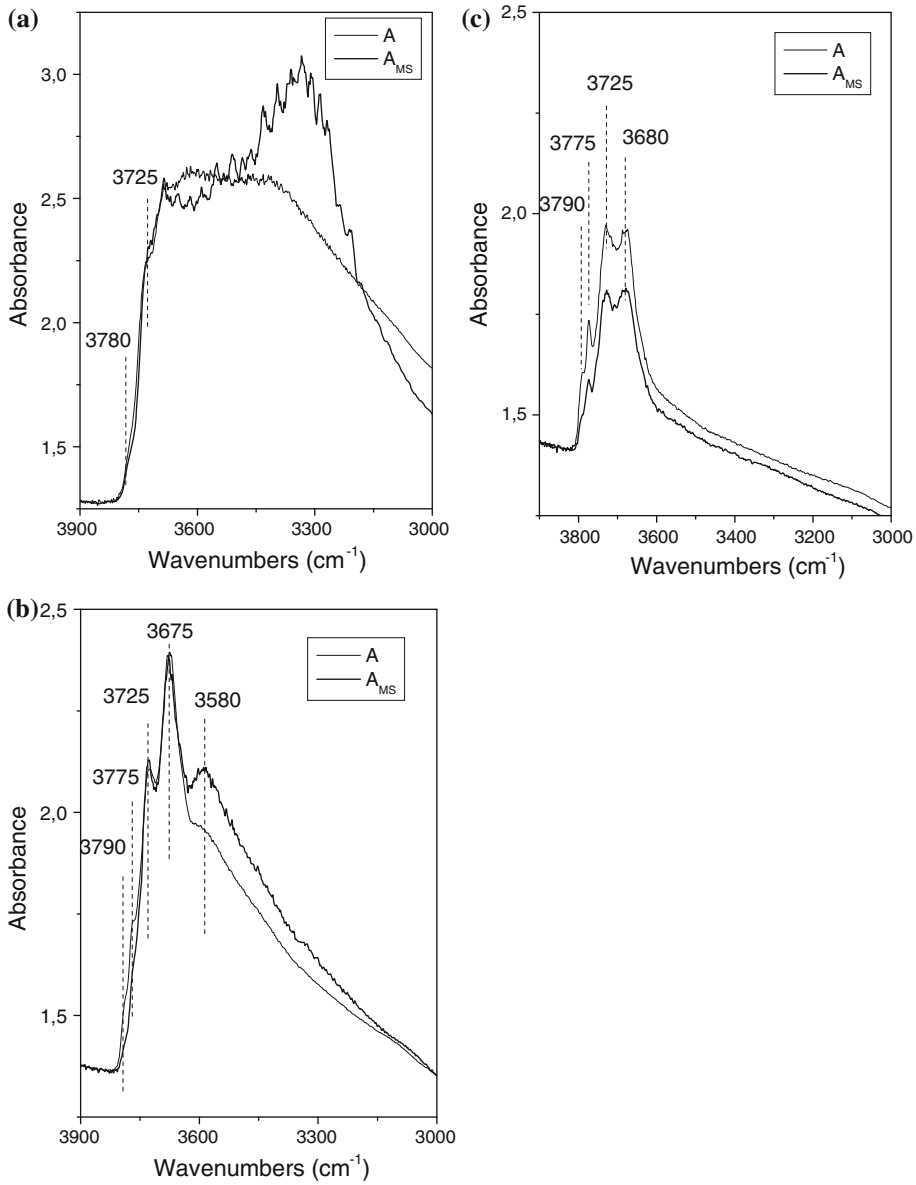

Fig. 8 Normalized FT-IR spectra recorded on samples A and A_{MS} out-gassed and 150 °C (**a**), 350 °C (**b**) and 500 °C (**c**)

new stronger Lewis sites (coordinatively unsaturated Al^{3+} ions). The band of CO interacting with OH species is seen to shift with coverage from 2160 to 2152 cm^{-1} due to the presence of several hydroxyls with different acidity, as shown in Fig. 8b.

With sample A outgassed at 500 °C (Fig. 9c), bands are seen of CO adsorbed on an Al^{3+} sites forming an extended phase (band at 2198 cm^{-1} shifting with coverage to 2183 cm^{-1}) and on residual hydroxyls (band at 2160 cm^{-1} shifting with coverage to 2156 cm^{-1}).

The relative intensities of bands due to CO adducts with Al^{3+} ions and OH species changed with the hydration degree of the surface, since new coordinatively unsaturated sites become available at the expenses of hydroxyls removed at higher temperature.

Figure 10 shows corresponding spectra recorded in same conditions, i.e. under the same equilibrium CO pressures, on sample A_{MS} pre-treated in the same way. As a whole, the same surface species were observed, i.e. coordinatively unsaturated Al^{3+} ions and surface hydroxyls, but with the following relevant differences:

(i) with A_{MS} outgassed at 150 °C (Fig. 10a), at low coverage the band of CO H-bonded to hydroxyls is seen at 2154 cm^{-1}, whereas at higher CO equilibrium pressures another component is seen at 2149 cm^{-1}. The difference with respect to the corresponding band on sample A outgassed at the same temperature is better shown in Fig. 10b, reporting spectra recorded on samples A and A_{MS} under the same CO pressure

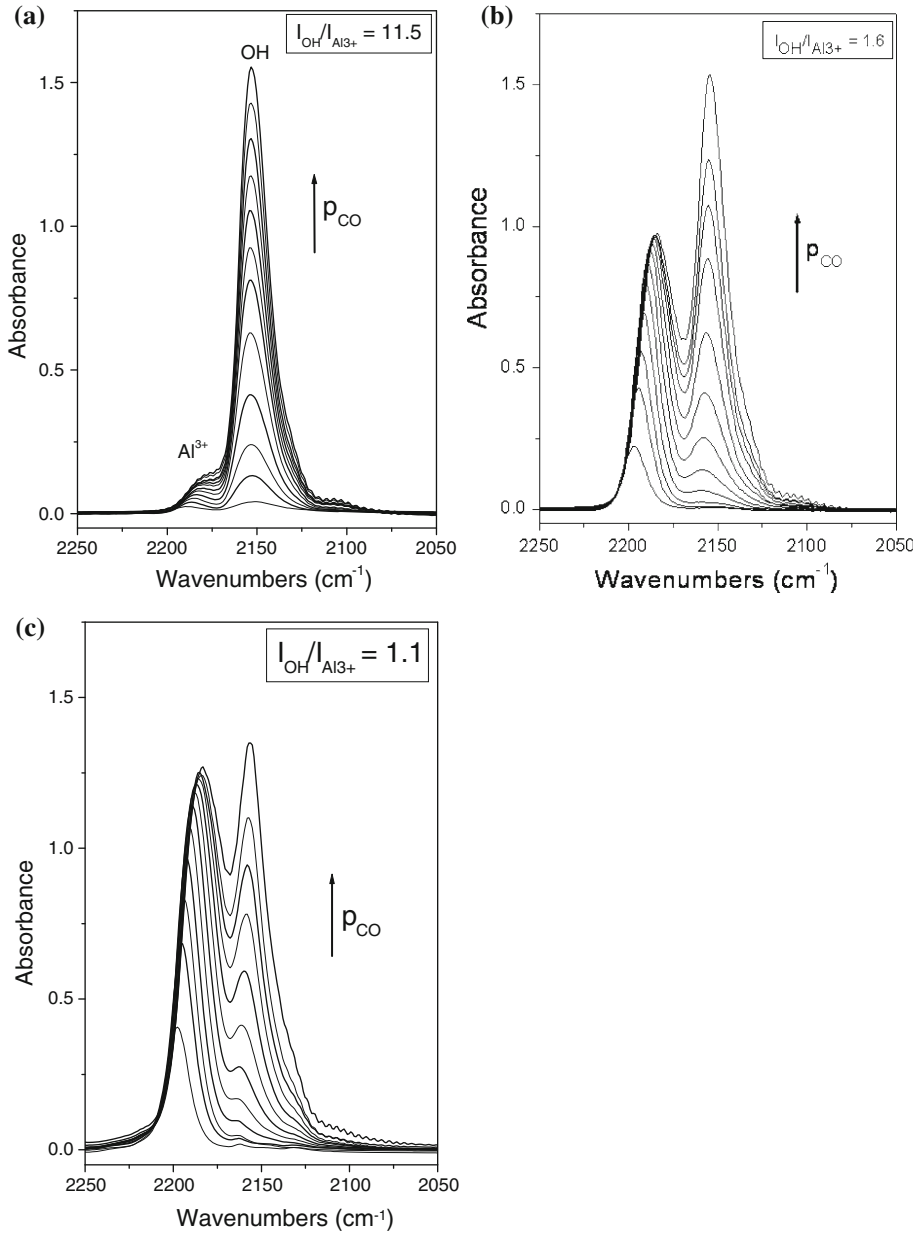

Fig. 9 FT-IR difference spectra, in the CO stretch region 2250–2050 cm^{-1} recorded after dosing CO on sample A outgassed at 150 °C (**a**), 350 °C (**b**) and 500 °C (**c**). CO equilibrium pressures range: 0.5–20 mbar; difference spectra obtained by subtracting spectra of bare sample reported in Fig. 6

(10 mbar). The smaller shift with respect to the free molecule mode (2143 cm^{-1}) indicates that the component at 2149 cm^{-1} should be related to CO interacting with weaker acidic hydroxyls, like those originally absorbing at 3330 cm^{-1} (Fig. 8a), stemming from the hydroxide phase (gibbsite);

(ii) normalized spectra recorded under the same CO equilibrium pressures allow us to draw some semi-quantitative observation: with A_{MS}, intensities of CO bands are always smaller than with A, indicating a smaller amount of sites actually accessible at the surface. The ratio $I_{OH}/I_{Al^{3+}}$, reported for each experiment, between intensities of the bands due to CO–HO and CO–Al^{3+} adducts, respectively, may be used to evaluate the relative abundance of Lewis and Brønsted sites. After treatment at 150 °C, $I_{OH}/I_{Al^{3+}}$ is 11.5 and 10.1 for A and A_{MS}, respectively: this can be explained by the fact that 3330 cm^{-1} hydroxyls belonging to gibbsite, though abundant, are less acidic and less prone to interact with CO; after treatment at 350 °C, $I_{OH}/I_{Al^{3+}}$ is 1.6 and 2.0 for A and A_{MS}, respectively, since A_{MS} surface is more hydrated, due to prolonged stirring in water. After outgassing at 500 °C, $I_{OH}/I_{Al^{3+}}$ is the same for both materials, due to the formation of the same γ-Al_2O_3 phase, according to Eq. 2.

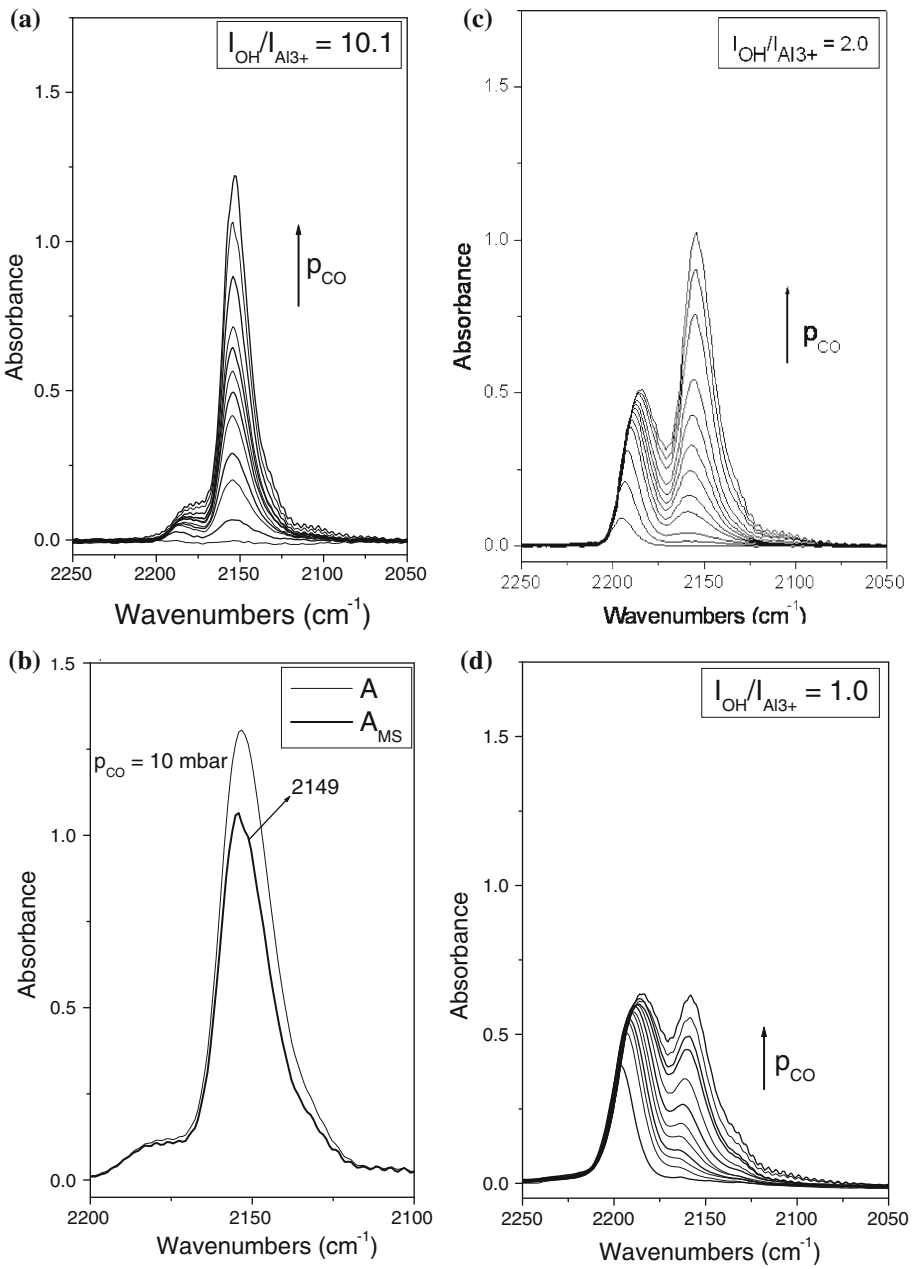

Fig. 10 FT-IR difference spectra, in the CO stretch region 2250–2050 cm^{-1}, recorded after dosing CO (equilibrium pressures in the 0.5–20 mbar range) on sample A_{MS} outgassed at 150 °C (**a**), 350 °C (**c**) and 500 °C (**d**). Difference spectra obtained by subtracting spectra of bare sample reported in Fig. 7. **b** Comparison of difference spectra recorded at the same CO equilibrium pressure (10 mbar) on samples A and A_{MS} outgassed at 150 °C

Conclusions

In this work, the study of the effect of magnetic stirring on nanometric transition alumina was carried out by complementary techniques in the field of materials science and surface physical-chemistry. It was therefore possible to figure out several differences concerning not only powder de-agglomeration, but also its surface properties, i.e. parameters that could affect important macroscopic behaviour, like the sinterability of the material or any potential catalytic application.

The comparison between A and A_{MS} showed that the magnetic stirring procedure deeply decreases the starting agglomerates size, but also affects the physico-chemical properties of the material. On one hand, the formation of an $Al(OH)_3$ (gibbsite) phase in A_{MS} was detected by XRD, indicating that a portion of the material, at least observable by XRD, was modified under stirring; on the other hand, by means of FT-IR spectroscopy it was possible to study surface functionalities. Normalized spectra of powders outgassed at 500 °C showed that stronger basic sites are present at the surface of A_{MS} (stable carbonates) and that changes occurred in the hydroxyls population.

The surface of A_{MS} was indeed more hydrated and less acidic OH species (band at 3300 cm^{-1}) were observed: such species were ascribed to the presence of a hydroxide

phase, which decomposed by increasing the temperature, in fair agreement with DTA–TG curves. Interestingly, such hydroxide phase did not form on a blank sample suspended in water without stirring, so pointing out the crucial role of magnetic stirring in the modification of the surface properties of the material.

References

1. Lippens BC, Steggerda JJ (1970) In: Linsen BG (ed) Physical and chemical aspects of adsorbents and catalysts. Academic Press, New York, p 171
2. Morterra C, Magnacca G (1996) Catal Today 27:497 (and references therein)
3. Mayo MJ (1996) Int Mater Rev 41:85
4. Teleki A, Wengeler R, Wengeler L, Nirschl H, Pratsinin SE (2008) Powder Technol 181:292
5. Bowen P, Carry C (2002) Powder Technol 128:248
6. Ma J, Lim LC (2002) J Eur Ceram Soc 22:2197
7. Bowen P, Carry C, Luxembourg D, Hofmann H (2005) Powder Technol 157:100
8. Bloch B, Ravi BG, Chaim R (2000) Mater Lett 42:61
9. Palmero P, Bonelli B, Lomello F, Garrone E, Montanaro L (2009) J Therm Anal Calorim 97:223
10. Palmero P, Lombardi M, Montanaro L, Azar M, Chevalier J, Garnier V (2009) Int J Appl Ceram Technol 6:420
11. Lefèvre G, Duc M, Lepeut P, Caplain R, Fédoroff M (2002) Langmuir 18:7530
12. Knözinger H, Ratnasamy P (1978) Catal Rev Sci Eng 17:31
13. Euzen P, Raybaud P, Krokidis X, Toulhoat H, Le Loarer JL, Jolivet JP, Froidefond C (2002) In: Schüth F, Sing KSW, Weitkamp J (eds) Handbook of porous solids, vol 3. Wiley-VCH, Weinheim, p 1591
14. Huang CC, Kono HO (1989) Ind Eng Chem Res 28:910
15. Mieth JA, Huang YJ, Schwarz JA (1988) J Colloid Interface Sci 123:366
16. Santacesaria E, Carra S, Adami I (1977) Ind Eng Chem Prod Res Dev 16(1):41
17. Digne M, Sautet P, Raybaud P, Euzen P, Toulhoat H (2004) J Catal 226:54
18. Chen Y, Hyldtoft J, Jacobsen CJH, Nielsen OF (1995) Spectrochim Acta A 51:2161
19. Dyer C, Hendra PJ, Forsling W, Ranheimer M (1993) Spectrochim Acta A 49:691
20. Laiti E, Persson P, Öhman LO (1998) Langmuir 14:825
21. Carrier X, Marceau E, Lambert J-F, Che M (2007) J Colloid Interface Sci 308:429
22. Reid CB, Forrester JS, Goodshaw HJ, Kisi EH, Suaning GJ (2008) Ceram Int 34:1551
23. Xie Z-P, Lu J-W, Huang Y, Cheng Y-B (2003) Mater Lett 57:2501
24. Sen S, Ram ML, Roy S, Sarkar BK (1999) J Mater Res 14:841
25. Gaydardzhiev S, Ay P (2006) J Mater Sci 41:5257. doi:10.1007/s10853-006-0354-7
26. Zhao W, Yang D, Song J, Yang Z, Liang C, Xu M, Xu T (2004) J Wuhan Univ Technol 19:4
27. Roelofs F, Vogelsberger W (2006) J Colloid Interface Sci 303:450
28. Kao H-C, Wei W-C (2000) J Am Ceram Soc 83:362
29. Azar M, Palmero P, Lombardi M, Garnier V, Montanaro L, Fantozzi G, Chevalier J (2008) J Eur Ceram Soc 28:1121
30. Hofmeister H, Kodderitzsch P, Dutta J (1998) J Non-Crystal Solids 232:182
31. Iordan A, Zaki MI, Kappenstein C (2004) Phys Chem Chem Phys 6:2502
32. Tsyganenko AA, Filimonov VN (1972) Spectrosc Lett 5:477
33. Tsyganenko AA, Filimonov VN (1973) J Mol Struct 19:579
34. Peri JB (1965) J Phys Chem 69:231
35. Busca G, Lonrenzelli V, Sanchez Escribano V, Guidetti R (1991) J Catal 131:167
36. Wang S-L, Johnston CT (2000) Am Mineral 85:739
37. Zecchina A, Areán CO (1996) Chem Rev 25(3):187 (and references therein)
38. Bonelli B, Onida B, Chen JD, Galarneau A, Di Renzo F, Fajula F, Garrone E (2004) Micropor Mesopor Mater 67:95
39. Lercher JA, Gründling C, Eder-Mirth G (1996) Catal Today 27:353
40. Cairon O, Chevreau T, Lavalley J-C (1998) J Chem Soc Faraday Trans 94:3039
41. Hadjiivanov KI, Vayssilov GN (2007) Adv Catal 47:307
42. Areán CO, Manoilova OV, Tsiganenko AA, Palomino GT, Mentruit MP, Geobaldo F, Garrone E (2001) Eur J Inorg Chem 7:1739
43. Morterra C, Bolis V, Magnacca G (1994) Langmuir 10:1812
44. Bolis V, Cerrato G, Magnacca G, Morterra C (1998) Thermochim Acta 321:63